IEEE Access
Multidisciplinary ⋮ Rapid Review ⋮ Open Access Journal

Received February 27, 2020, accepted March 21, 2020, date of publication March 26, 2020, date of current version April 13, 2020.

Digital Object Identifier 10.1109/ACCESS.2020.2983490

Analysis and Design of Generalized Class-E/F_2 and Class-E/F_3 Inverters

JINGYUE MA[1], ASIYA[1], (Student Member, IEEE), XIUQIN WEI[2], (Member, IEEE), KIEN NGUYEN[1], (Senior Member, IEEE), AND HIROO SEKIYA[1], (Senior Member, IEEE)

[1]Graduate School of Science and Engineering, Chiba University, Chiba 263-8522, Japan
[2]Department of Electrical Engineering, Chiba Institute of Technology, Narashino 275-0016, Japan

Corresponding author: Hiroo Sekiya (sekiya@facultychiba-u.jp)

This work was supported by the RIEC Nation-Wide Cooperative Research Projects at Tohoku University under Grant H30/B12.

ABSTRACT This paper presents analytical expressions of the class-E/F_n inverter with generality. The characteristics of the class-E/F_2 and class-E/F_3 inverters can be comprehended in a theoretical manner by using the analytical expressions. In-depth investigations are provided in terms of the power output capability. By investigating the entire parameter spaces, the design strategy for achieving high power output capability is given. In addition, the characteristics of the class-Φ_2 and class-Φ_3 inverters, which are special modes of the class-E/F_2 and class-E/F_3 inverters, respectively, are shown. The experimental and PSpice-simulation results agreed with analytical predictions quantitatively, which showed the validities of the analytical expressions and characteristic investigations in this paper.

INDEX TERMS Class-E/F_2 inverter, class-E/F_3 inverter, class-Φ_2 inverter, class-Φ_3 inverter, power-output capability, output power.

I. INTRODUCTION

With the requirement for the efficient operation of the power-supply circuit at high-frequency, The designs and constructions of high-frequency dc/ac inverters and amplifiers are increasing importance. The class-E inverter [1]–[7] is widely known as a high-frequency resonant inverter that can work at megahertz-order frequencies with high power-conversion efficiency. That is because the class-E inverter achieves the zero-voltage switching (ZVS) and zero-derivative voltage switching (ZDS). The main disadvantage of the class-E inverter is, however, its high peak of the switch voltage, which is approximately 3.6 times as high as the input voltage at a 50 % duty ratio. This switch stress is higher than those of the class-D and class-F inverters [1], [2], [8].

By adding a harmonic resonant filter to the output resonant filter of the class-E inverter, it is possible to reduce the switch voltage and current stresses [9]–[18]. The class-E/F_n inverter has a $n-$th harmonic series resonant filter, which is connected to the switching device in parallel. Table 1 gives a survey of the previous papers, which describes the class-E/F_n inverters. In [12], the characteristics of the class-E/F_2 inverter in terms of the power output capability were investigated. A global maximum power output capability was obtained in the parameter space of the quality factor of the harmonic-resonant filter Q_n and the switch duty ratio D. In [13], the characteristics between the class-E/F_2 and class-E/F_3 inverters were compared at any duty ratio. Both [12] and [13] evaluated the inverter characteristics under the conditions of high input inductance L_I and high quality factor of the output-resonant filter Q_0. In [14], design equations were derived for the class-E/F_3 inverter with the assumptions that Q_n and Q_0 are high and the duty ratio is 0.5. However, this paper has not shown any circuit performance of the class-E/F_3 inverter.

The class-E/F_n inverter can satisfy the class-E ZVS/ZDS conditions even if L_I is low [15]–[18]. The typical such type of inverter is the class-Φ_n inverter. The definition of the class-Φ_n inverter is the class-E/F_n inverter with no reactance component in the output resonant filter. In this sense, the class-Φ_n inverter belongs to the class-E/F_n inverter family. The class-Φ_n inverters have been designed by transforming the output resonant filter from the class-E/F_n inverter with high Q_0 and high L_I. Because of the transformation of the output filter inductance, the class-E/F_n inverter with low L_I can be designed [18]. However, there is no analytical waveform equation of the generalized class-E/F_n inverter, namely the class-E/F_n inverter with consideration of any D,

The associate editor coordinating the review of this manuscript and approving it for publication was Dušan Grujić.

TABLE 1. Survey of the class-E inverter with harmonic resonance.

Reference	Inverter type	L_I	Q_n	Q_0	D	Analytical equations
12	Class-E/F$_2$	High	Any	High	Any	Yes
13	Class-E/F$_{2,3}$	High	High	High	Any	Yes
14	Class-E/F$_3$	High	High	High	0.5	Yes
18	Class-Φ_2	Low	Low	Low	0.5	No
This paper	Class-E/F$_{2,3}$ Class-$\Phi_{2,3}$	Any	Any	Any	Any	Yes

L_I, Q_n, and Q_0. This is because much harmonic component is included in every inductance current, which increases analysis complexity and difficulty. It is necessary to have analytical waveform equations for obtaining the theoretical output power capability in the entire parameter spaces.

This paper proposes the analysis method for deriving the waveform-equation of the generalized class-E/F$_n$ inverters. In addition, the characteristics of the class-E/F$_2$ and E/F$_3$ inverters are comprehended in a theoretical manner by using the analytical waveform equations. The presented analytical expressions are valid for any D, L_I, Q_n, and Q_0. Therefore, it is possible to investigate the effects of these parameters on the circuit characteristics quickly with low computation cost. The design strategies of the inverters for achieving the highest power output capability and the highest output power are shown. Furthermore, the characteristics of the class-Φ_2 and class-Φ_3 inverters are also clarified. From the theoretical evaluations, we can show that:

1. The duty ratio for obtaining the maximum power output capability of the class-E/F$_2$ inverter is $D = 0.375$.
2. The class-E/F$_2$ inverter can achieve the highest power output capability $c_p = 0.133$ even if the input inductance L_I is low.
3. The class-Φ_2 inverter works with high output capability $c_p = 0.132$ and the highest output power of the class-E/F$_2$ inverter.
4. In the class-E/F$_3$ inverter, the duty ratio for obtaining the maximum power output capability is $D = 0.575$.
5. By investigating entire parameter ranges, this paper discovers a parameter set for obtaining the highest power output capability $c_p = 0.144$. This value is higher than the known maximum value of $c_p = 0.135$.
6. The class-Φ_3 inverter is one of the best-performed class-E/F$_3$ inverter in the sense of high output capability $c_p = 0.143$ and the highest output power.

The circuit experiments were carried out for four types of inverters. It was confirmed that all the experimental and PSpice-simulation waveforms agreed with the analytical predictions quantitatively, which showed the validities of the analytical expressions and the characteristics evaluations.

II. CIRCUIT TOPOLOGY AND THE OPERATION PRINCIPLE

Figure 1 shows a circuit-topology of the class-E/F$_n$ inverter. The circuit topology of the class-E/F$_2$ inverter is the same as that of the class-E/F$_3$ inverter. The inverter consists of input direct-voltage source V_I, input inductance L_I, switch device S with a shunt capacitance C_S, and output-resonant filter L_0-C_o-R, which are the same as the class-E inverter. The class-E/F$_n$ inverter has a *n-th* harmonic series-resonant filter L_n-C_n, which is connected to the switch device in parallel.

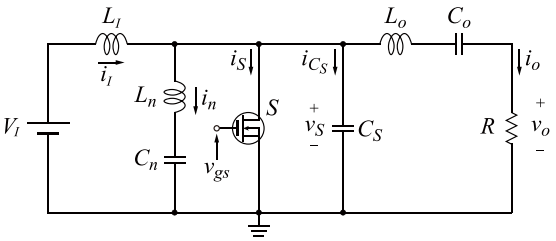

FIGURE 1. Circuit topology of the class-E/F$_n$ inverter.

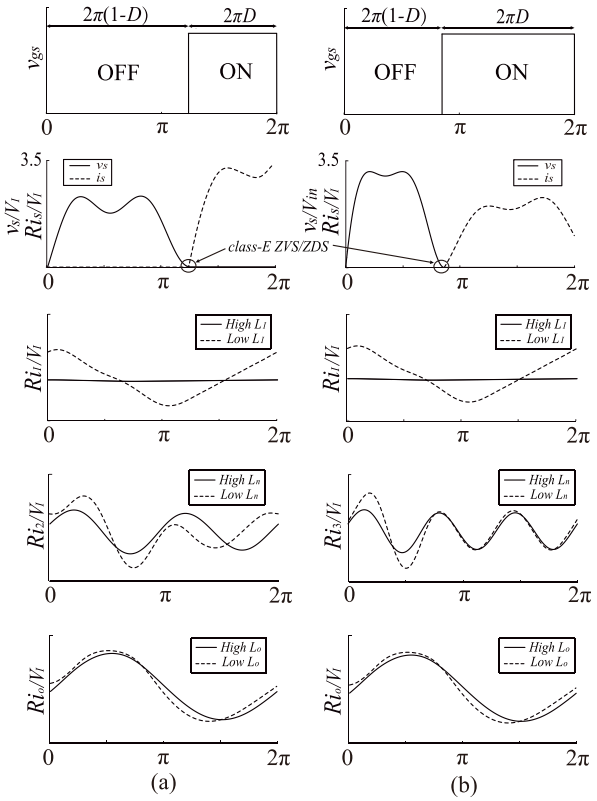

FIGURE 2. Example waveforms. (a) Class-E/F$_2$ inverter. (b) Class-E/F$_3$ inverter.

Figure 2 shows example waveforms of the class-E/F$_n$ inverters. The driving voltage v_{gs} drives the MOSFET with a switch-on duty ratio D. In the class-E/F$_n$ inverter, three inductances L_I, L_n, and L_0 in Fig. 1 have a role to determine the circuit characteristics individually. If the input inductance L_I is high, the input current i_I is regarded as the direct current as shown in Fig. 2. Conversely, a large current ripple appears in case of low L_I. When the quality factor of the harmonic filter Q_n and that of the output filter Q_0 are high, the currents flowing through the harmonic filter and the output filter are purely sinusoid. Basically, high Q-value can be obtained when the resonant inductance is high and resonant capacitance is low.

The non-sinusoidal currents, however, occur in case of low Q as shown in Fig. 2.

The harmonic resonant filter L_n-C_n resonates at $n-$th harmonic frequency [13], [17], [19], [20]. Generally, high L_I and the high Q_0 network refuse the harmonic-resonant current to flow through their branches. Namely, most harmonic current flows into the switch or the shunt capacitance. When the switch is in the off-state, the current flowing through the shunt capacitance produces the switch voltage v_S. By adding the harmonic resonant filter, the peak value of the switch voltage can be reduced compared with the class-E inverter. Because of the harmonic current, the square wave-like switch voltage v_S can be obtained as shown in Fig. 2. The peak values of the switch voltage of the class-E/F_2 and class-E/F_3 inverters are typically 2.2 and 3.2 times as high as the input voltage, respectively, which are lower than that of the class-E inverter.

When the switch turns on at $\omega t = 2\pi(1-D)$, the switch voltage $v_S(\omega t)$ satisfies the class-E ZVS/ZDS conditions as shown in Fig. 2, which are expressed as

$$v_S(2\pi(1-D)) = 0, \tag{1}$$

$$\left.\frac{dv_S(\omega t)}{d\omega t}\right|_{\omega t=2\pi(1-D)} = 0. \tag{2}$$

The class-E ZVS/ZDS minimizes the switching loss, which can provide the megahertz-order frequency operation with high efficiency.

In the fundamental designs of the class-E/F_n inverters, namely at high L_I, the inductive output network is mandatory for achieving the class-E ZVS/ZDS conditions [12], [13], [17], [18]. For achieving the class-E ZVS/ZDS, it is necessary to adjust the phase shift between the switching timing and the output current. By decreasing the value of L_I, however, a non-negligible input-current ripple occurs as shown in Fig. 2. The ripple size can adjust the current waveform flowing through the shunt capacitance. Therefore, it is possible to satisfy the class-E ZVS/ZDS conditions even though the resonant frequency of the output filter is close to the operating frequency. When the resonant frequency is the same as the operating frequency, the class-E/F_n inverter is specially called the class-Φ_n inverter [15]–[18].

III. ANALYTICAL WAVEFORM DERIVATION

The main purpose of this paper is to investigate the circuit characteristics of the generalized class-E/F_n inverters at any D, L_I, Q_n, and Q_0. For evaluating the inverter characteristics theoretically, it is necessary to derive the waveform equations with generality.

A. ASSUMPTION

The analytical waveforms and the inverter-characteristic evaluations are based on the following assumptions.

1. All the inductances and capacitances have no parasitic resistance.
2. The MOSFET works ideally. Therefore, zero-switching time, zero on-resistance, and infinite off-resistance are assumed. From assumptions 1 and 2, no power loss occurs in the inverter.
3. The MOSFET turns off at $\theta = 0$. Namely, the MOSFET is in the off-state for $0 < \omega t \leq 2\pi(1-D)$, and in on state for $2\pi(1-D) < \omega t \leq 2\pi$.
4. The shunt capacitance C_S includes the MOSFET drain-to-source capacitance.
5. All the passive components including the MOSFET drain-to-source capacitance work as linear elements.
6. The harmonic resonant frequency is the same as the harmonic operating frequency. Therefore, we have

$$n\omega = \frac{1}{\sqrt{L_n C_n}}. \tag{3}$$

B. WAVEFORM EQUATIONS

First, we express the normalized currents flowing through input inductance, harmonic resonant inductance, and output resonant inductance as

$$\frac{Ri_I}{V_I} = a_{i0} + \sum_{k=1}^{N}[a_{ik}\cos(k\omega t) + b_{ik}\sin(k\omega t)], \tag{4}$$

$$\frac{Ri_n}{V_I} = \sum_{k=1}^{N}[a_{nk}\cos(k\omega t) + b_{nk}\sin(k\omega t)], \tag{5}$$

$$\frac{Ri_o}{V_I} = \sum_{k=1}^{N}[a_{ok}\cos(k\omega t) + b_{ok}\sin(k\omega t)], \tag{6}$$

respectively, where N is the maximum value of the considered harmonic component number. We set $N = 8$ in this paper. From the KCL, we have a basic equation as

$$i_I = i_n + i_o + i_S + i_{CS}. \tag{7}$$

In the switch-off state, namely $0 \leq \omega t < 2\pi(1-D)$, the normalized current flowing through the MOSFET and the shunt capacitance can be obtained as

$$\frac{Ri_S}{V_I} = 0, \tag{8}$$

and

$$\begin{aligned}\frac{Ri_{CS}}{V_I} &= \frac{R}{V_I}(i_I - i_n - i_o)\\ &= a_{i0} + \sum_{k=1}^{N}[(a_{ik} - a_{nk} - a_{ok})\cos(k\omega t)\\ &\quad + (b_{ik} - b_{nk} - b_{ok})\sin(k\omega t)],\end{aligned} \tag{9}$$

respectively. The current flowing throught the shunt capacitance produces the switch voltage v_S, namely

$$\begin{aligned}\frac{v_S}{V_I} &= \frac{1}{\omega C_S R}\int_0^{\omega t}\frac{Ri_{CS}}{V_I}d(\omega t)\\ &= \frac{1}{\omega C_S R}\left\{a_{i0}\omega t + \sum_{k=1}^{N}\frac{1}{k}[(a_{ik} - a_{nk} - a_{ok})\sin(k\omega t)\right.\\ &\quad \left. - (b_{ik} - b_{nk} - b_{ok})\cos(k\omega t) + (b_{ik} - b_{nk} - b_{ok})]\right\}.\end{aligned} \tag{10}$$

When the switch is in the on-state, namely $2\pi(1-D) \le \omega t < 2\pi$, the normalized current flowing through the MOSFET and the shunt capacitance are expressed as

$$\begin{aligned}\frac{Ri_S}{V_I} &= \frac{R}{V_I}(i_I - i_n - i_o)\\ &= a_{i0} + \sum_{k=1}^{N}[(a_{ik} - a_{nk} - a_{ok})\cos(k\omega t)\\ &\quad + (b_{ik} - b_{nk} - b_{ok})\sin(k\omega t)],\end{aligned} \tag{11}$$

and

$$\frac{Ri_{CS}}{V_I} = 0, \tag{12}$$

respectively. The ZVS condition prevents the instant discharging at the shunt capacitance C_S. In addition, the normalized switch voltage during swtich on-state is

$$\frac{v_S}{V_I} = 0. \tag{13}$$

From the above, the normalized switch voltage and current waveforms are

$$\frac{v_S}{V_I} = \begin{cases} \dfrac{1}{\omega C_s R}\Big\{a_{i0}\omega t + \displaystyle\sum_{k=1}^{N}\frac{1}{k}[(a_{ik} - a_{nk} - a_{ok})\sin(k\omega t)\\ -(b_{ik} - b_{nk} - b_{ok})\cos(k\omega t) + (b_{ik} - b_{nk} - b_{ok})]\Big\}, \\ \qquad\qquad \text{for } 0 < \omega t \le 2\pi(1-D)\\ 0, \qquad\qquad \text{for } 2\pi(1-D) < \omega t \le 2\pi \end{cases} \tag{14}$$

$$\frac{Ri_S}{V_I} = \begin{cases} 0, \qquad\qquad \text{for } 0 < \omega t \le 2\pi(1-D)\\ a_{i0} + \displaystyle\sum_{k=1}^{N}[(a_{ik} - a_{nk} - a_{ok})\cos(k\omega t)\\ +(b_{ik} - b_{nk} - b_{ok})\sin(k\omega t)].\\ \qquad\qquad \text{for } 2\pi(1-D) < \omega t \le 2\pi \end{cases} \tag{15}$$

C. DERIVATIONS OF INDUCTANCE-CURRENT COEFFICIENTS

By applying the Fourier series expansion to Eq.(15), we have

$$\frac{v_S}{V_I} = c_0 + \sum_{k=1}^{N}[c_k\cos(k\omega t) + d_k\sin(k\omega t)]. \quad \text{for } 0 < \omega t \le 2\pi \tag{16}$$

The resulting equations of c_0, c_k, and d_k are the functions of the inductance-current coefficients as given in Appendix A.

Figure 3 shows the equivalent circuit of the inverter. The equivalent circuit has three loops as shown in Fig. 3. By considering the KVL of each loop, we obtain three types of the normalized switch voltage expressions as

$$\begin{aligned}\frac{v_S}{V_I} &= 1 - \frac{\omega L_I}{R}\frac{d(Ri_I/V_i)}{d(\omega t)},\\ &= 1 + \frac{\omega L_I}{R}\sum_{k=1}^{N} k\big[a_{ik}\sin(k\omega t) - b_{ik}\cos(k\omega t)\big],\end{aligned} \tag{17}$$

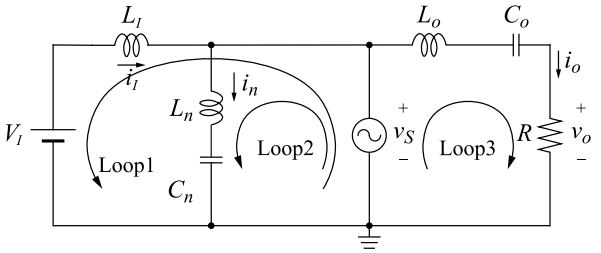

FIGURE 3. Equivalent circuit model.

$$\begin{aligned}\frac{v_S}{V_I} &= \frac{\omega L_n}{R}\frac{d(Ri_n/V_i)}{d(\omega t)} + \frac{1}{\omega C_n R}\int_0^{\omega t}\frac{Ri_n}{V_I}d(\omega t),\\ &= \frac{\omega L_n}{R}\sum_{k=1}^{N} k[-a_{nk}\sin(k\omega t) + b_{nk}\cos(k\omega t)]\\ &\quad + \frac{1}{\omega C_n R}\sum_{k=1}^{N}\frac{1}{k}[a_{nk}\sin(k\omega t) - b_{nk}\cos(k\omega t)],\end{aligned} \tag{18}$$

$$\begin{aligned}\frac{v_S}{V_I} &= \frac{\omega L_0}{R}\frac{d(Ri_o/V_i)}{d(\omega t)} + \frac{1}{\omega C_o R}\int_0^{\omega t}\frac{Ri_o}{V_I}d(\omega t) - \frac{Ri_o}{V_I},\\ &= \frac{\omega L_0}{R}\sum_{k=1}^{N} k[-a_{ok}\sin(k\omega t) + b_{ok}\cos(k\omega t)]\\ &\quad + \frac{1}{\omega C_o R}\sum_{k=1}^{N}\frac{1}{k}[a_{ok}\sin(k\omega t) - b_{ok}\cos(k\omega t)]\\ &\quad + \sum_{k=1}^{N}[a_{ok}\cos(k\omega t) + b_{ok}\sin(k\omega t)].\end{aligned} \tag{19}$$

From the coefficient comparisons between (16) and (17)-(19), $(6N+1)$ algebraic equations can be obtained, namely

$$\begin{cases} c_0 - 1 = 0,\\ c_k + \dfrac{k\omega L_I}{R}b_{ik} = 0,\\ d_k - \dfrac{k\omega L_I}{R}a_{ik} = 0,\\ c_k - \dfrac{k\omega L_n}{R}b_{nk} + \dfrac{1}{k\omega C_n R}b_{nk} = 0,\\ d_k + \dfrac{k\omega L_n}{R}a_{nk} - \dfrac{1}{k\omega C_n R}a_{nk} = 0,\\ c_k - \dfrac{k\omega L_o}{R}b_{ok} + \dfrac{1}{k\omega C_o R}b_{ok} - a_{ok} = 0,\\ d_k + \dfrac{k\omega L_o}{R}a_{ok} - \dfrac{1}{k\omega C_o R}a_{ok} - b_{ok} = 0.\\ \qquad \text{for } k = 1, 2, \cdots N \end{cases} \tag{20}$$

In this paper, we evaluate the inverter characteristics for satisfying the class-E ZVS/ZDS conditions in (1) and (2). Therefore, it is necessary to solve $(6N+3)$ algebraic equations simultaneously. There are $(6N+9)$ unknown parameters, which are $a_{i0}, a_{ik}, b_{ik}, a_{nk}, b_{nk}, a_{ok}, b_{ok}, \omega L_I/R$, $\omega L_o/R$, $\omega L_n/R$, $\omega C_0 R$, $\omega C_n R$, $\omega C_S R$, D, and n, in the waveform equations. The number of unknown inductance-current coefficients is the same as that of the equations in (20). The harmonic resonance number n is given according to

the operation mode. When L_n is given, C_n is determined from (3). Therefore, when we give D, $\omega L_I/R$, $\omega L_0/R$, and $\omega L_n/R$, (1), (2), and (20) can be solved numerically and inductance-current coefficients, $\omega C_S R$, and $\omega C_0\ R$ are detrmined uniquely. The major challenge for the inverter design is how to give the parameters of D, $\omega L_I/R$, $\omega L_0/R$, and $\omega L_n/R$.

D. POWER OUTPUT CAPABILITY

In this paper, we adopt the power output capability for inverter characteristic evaluations. From the assumptions 1 and 2, the power output capability is expressed as

$$c_p = \frac{RP_o/V_I^2}{(v_{Smax}/V_I)(Ri_{Smax}/V_I)} = \frac{RI_I/V_I}{(v_{Smax}/V_I)(Ri_{Smax}/V_I)}. \tag{21}$$

where RP_o/V_I^2 is the normalized output power, which is expressed as

$$\frac{RP_o}{V_I^2} = \frac{1}{2\pi}\int_0^{2\pi}\left(\frac{Ri_o}{V_I}\right)^2 d(\omega t) = \frac{1}{2}\sum_{k=1}^{N}(a_{ok}^2 + b_{ok}^2), \tag{22}$$

and I_I is the average value of the normalized input current, which is expressed as

$$\frac{RI_I}{V_I} = \frac{1}{2\pi}\int_0^{2\pi}\frac{Ri_I}{V_I}d\omega t = a_{i0}. \tag{23}$$

In addition, v_{Smax} and i_{Smax} are the maximum value of the switch voltage and current, respectively. For deriving the output power capability, it is necessary to obtain v_{Smax}/V_I and Ri_{Smax}/V_I from the analytical waveforms. Both $v_S(1-2\pi D)$ and $v_S(2\pi)$ are zero when the class-E ZVS/ZDS conditions are satisfied. Therefore, v_{Smax}/V_I is the peak value of the normalized switch voltage during the off-state. The angular time for the peak switch-voltage appearance can be obtained by solving

$$\frac{1}{V_I}\frac{dv_S(\omega t)}{d\omega t} = 0, \quad \text{for } 0 < \omega t < 2\pi(1-D). \tag{24}$$

By substituting the obtained angular time into (10), v_{Smax}/V_I can be obtained.

Conversely, Ri_{Smax}/V_I appears during the on-state. Because of the class-E ZVS/ZDS, the switch current is zero at $\omega t = 2\pi(1-D)$. Similar to (24), the angular time for peak switch-current appearance can be obtained by solving

$$\frac{R}{V_I}\frac{di_S(\omega t)}{d\omega t} = 0, \quad \text{for } 2\pi(1-D) < \omega t < 2\pi. \tag{25}$$

By substituting the angular time into (11), the peak value of the normalized switch current is obtained. For deriving Ri_{Smax}/V_I, this peak value should be compared with Ri_S/V_I at $\omega t = 2\pi$. If there is no solution of ωt in (25), Ri_{Smax}/V_I becomes Ri_S/V_I at $\omega t = 2\pi$.

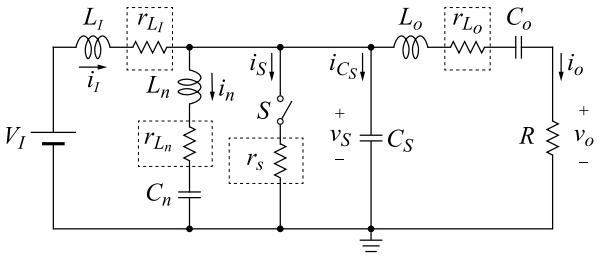

FIGURE 4. Power-loss model.

E. POWER-LOSS ANALYSIS

Figure 4 shows the power-loss model. In this paper, the power losses at the equivalent series resistances (ESRs) of the input, harmonic-resonant, and output-filter inductances, namely r_{LI}, r_{Ln}, and r_{L0}, respectively are considered. In addition, the conduction loss on the MOSFET on-resistance r_S is also taken into account. It is assumed in the power-loss analysis that the ESRs and switch on-resistance do not affect the inverter waveforms [4].

The total amount of the normalized power losses is

$$\frac{RP_{loss}}{V_I^2} = \frac{R}{V_I^2}\left(P_S + P_{LI} + P_{Ln} + P_{Lo}\right), \tag{26}$$

where RP_S/V_I^2 is the normalized conduction loss at r_S, RP_{LI}/V_I^2, RP_{Ln}/V_I^2, and RP_{Lo}/V_I^2 are the normalized power losses at r_{LI}, r_{Ln}, and r_{L0}, respectively. The concarete expressions of them are given in Appendix B. The power conversion efficiency is estimated from

$$\eta = \frac{RP_o/V_I^2}{RP_o/V_I^2 + RP_{loss}/V_I^2}. \tag{27}$$

IV. INVERTER CHARACTERISTIC INVESTIGATIONS

There are many parameter sets of the class-E/F_n inverters. The purposes of this section are to evaluate the parameter effects on the inverter characteristics, to derive the proper parameter set to obtain high power output capability, and to show a design strategy of the class-Φ_n inverters.

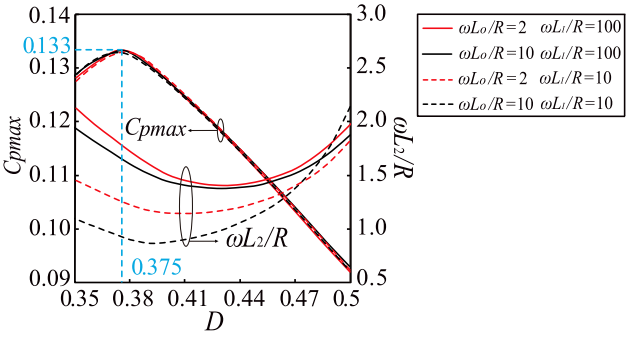

FIGURE 5. Maximum power output capability c_{pmax} of the class-E/F_2 inverter and $\omega L_2/R$ to obtain c_{pmax} for fixed $\omega L_I/R$ and $\omega L_0/R$ as a function of duty ratio.

A. CLASS-EF_2 INVERTER

Figure 5 shows the maximum value of the power output capability c_{pmax} and $\omega L_2/R$ to obtain c_{pmax} for fixed $\omega L_0/R$ and

$\omega L_I/R$ as a function of D. For drawing this figure, the $\omega L_0/R$ and the $\omega L_I/R$ are given firstly. After that, the $\omega L_2 R$ to obtain c_{pmax} for the given parameters is searched. It is seen from Fig. 5 that the highest values of c_{pmax} of the class-E/F$_2$ inverter are obtained around D=0.375 regardless of $\omega L_0/R$ and the $\omega L_I/R$. The value of $D = 0.375$ is also pointed out in [12] and [13]. In [12] and [13], however, the characteristics were evaluated under the conditions of high L_I and Q_0. It is a new knowledge that the value of $D = 0.375$, which is the duty ratio to obtain high power output capability, is independent of the $\omega L_I/R$ and the $\omega L_0/R$ even though these values are small. Because we would like to focus on how to design the inverter with high power output capability, the duty ratio is fixed as $D = 0.375$ in the following investigations.

1) MAXIMUM POWER OUTPUT CAPABILITY

For finding the parameter set to obtain the high power output capability, we investigated the effects of $\omega L_I/R$, $\omega L_2/R$, and $\omega L_0/R$.

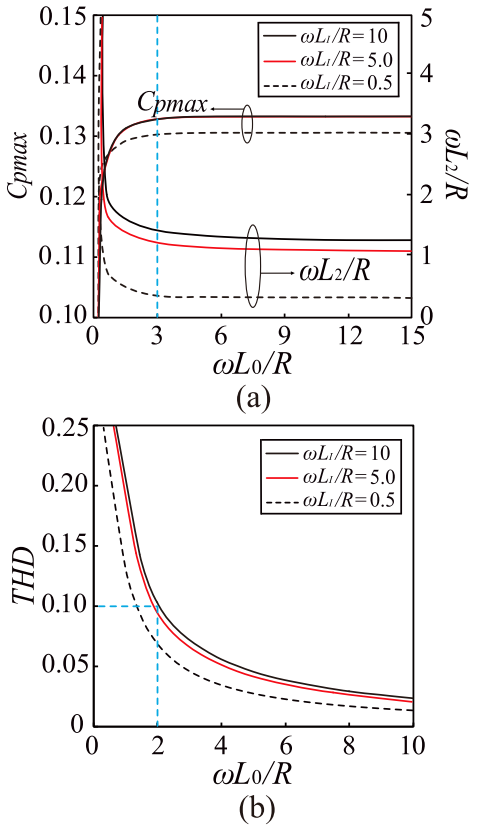

FIGURE 6. Characteristics of the class-E/F$_2$ inverter for fixed $\omega L_I/R$ as a function of the $\omega L_0/R$. (a) Maximum power output capability c_{pmax} and $\omega L_2/R$ to obtain c_{pmax}. (b) Total harmonic distortion of the output current.

Figure 6 shows the characteristics of the class-E/F$_2$ inverter for fixed $\omega L_I/R$ as a function of $\omega L_0/R$. It is seen from Fig. 6(a) that c_{pmax} is almost constant in the range of $\omega L_0/R > 3$. Additionally, this characteristic is independent of the $\omega L_I/R$. Figure 6(b) shows the total harmonic distortion (THD) of the output current as a function of the $\omega L_0/R$, where the THD is defined as

$$THD = \sqrt{\frac{\sum_{k=2}^{N}(a_{ok}^2 + b_{ok}^2)}{a_o^2 + b_o^2}}. \tag{28}$$

When the THD is less than 0.1, the output current is regarded as a pure sinusoidal waveform in this paper. It is seen from Fig. 6(b) that the THD is less than 0.1 in the range of $\omega L_0/R > 2$ regardless of $\omega L_I/R$. Namely, it can be stated that Q_0-value is sufficiently high in the range of $\omega L_0/R > 3$. From the above considerations, the output current is purely sinusoid when the highest value of c_p is obtained. In other words, c_p deteriorates drastically in case of low Q_0.

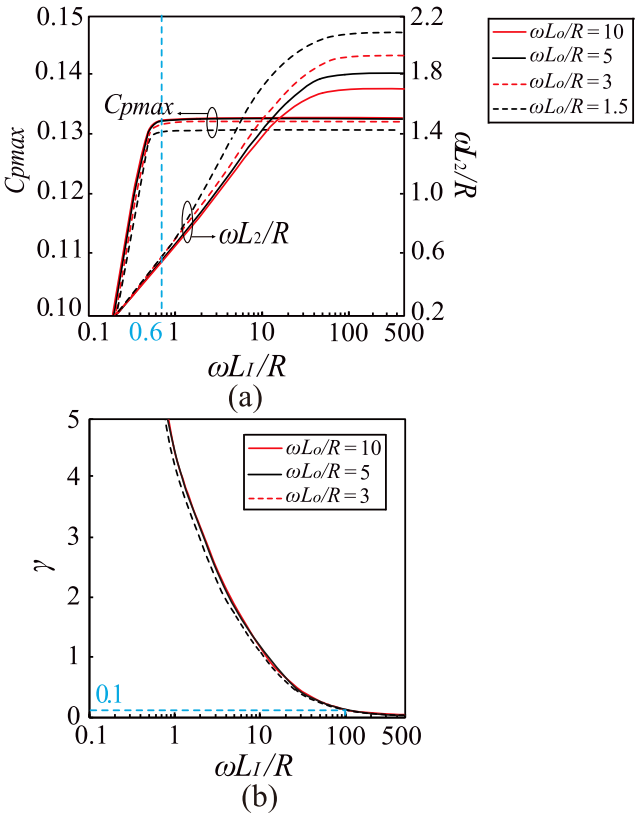

FIGURE 7. Characteristics of the class-E/F$_2$ inverter for fixed $\omega L_0/R$ as a function of the $\omega L_I/R$. (a) Maximum power output capability c_{pmax} and $\omega L_2/R$ to obtain c_{pmax}. (b) Ripple ratio of the input current.

Figure 7 shows the characteristics of the class-E/F$_2$ inverter for fixed $\omega L_0/R$ as a function of $\omega L_I/R$. It is seen from Fig. 7(a) that the maximum value of the output power capability is almost constant in the range of $\omega L_I/R > 0.6$. This characteristic is independent of $\omega L_0/R$. Figure 7(b) shows the ripple ratio of the input current γ as a function of the $\omega L_I/R$. The ripple ratio is defined as $\gamma = \Delta i_I/I_I$, where Δi is the peak-to-peak value of the input current. In the case of $\gamma < 0.1$, the input current is regarded as direct current in the paper. It is seen from Fig. 7(b) that γ is less than 0.1 in the range of $\omega L_I/R > 100$ regardless of the $\omega L_0/R$. Note that $c_p = 0.133$ can be obtained even though $\omega L_I/R$ is small.

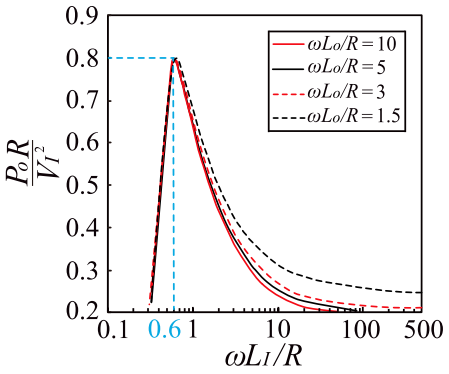

FIGURE 8. Normalized output power of the class-E/F$_2$ inverter to obtain the c_{pmax} for fixed $\omega L_0/R$ as a function of $\omega L_I/R$.

It is seen from Figs. 6(a) and 7(a) that the $\omega L_2/R$ to obtain c_{pmax} is in the range of $\omega L_2/R < 2$, which is regarded as low Q_2. Namely, the harmonic resonant current i_2 always includes other harmonic components when the class-E/F$_2$ inverter achieves $c_p = 0.133$.

From the above results, it is clarified that there are many parameter sets to obtain $c_p = 0.133$. When the $\omega L_0/R$ and the $\omega L_I/R$ are sufficiently large, $c_p = 0.133$ can be obtained. In this situation, we have $\omega L_2/R = 1.67$. This result is the same as the previous paper [12]. It is also clarified that we can have $c_p = 0.133$ at low L_I.

2) OUTPUT POWER AND CLASS-Φ_2 INVERTER

Figure 8 shows the normalized output power of the class-E/F$_2$ inverter to obtain c_{pmax} for fixed $\omega L_0/R$ as a function of the $\omega L_I/R$. It is seen from Fig. 8 that the output power has a peak value against the $\omega L_I/R$ variation. The largest power of $P_oR/V_I^2 = 0.8$ appears at $\omega L_I/R = 0.6$. From Fig. 7(a), we see that the maximum power output capability is $c_{pmax} = 0.132$ at $\omega L_I/R = 0.6$ for $\omega L_0/R > 3$, which is almost the same as the highest value of $c_p = 0.133$ in the class-E/F$_2$ inverter.

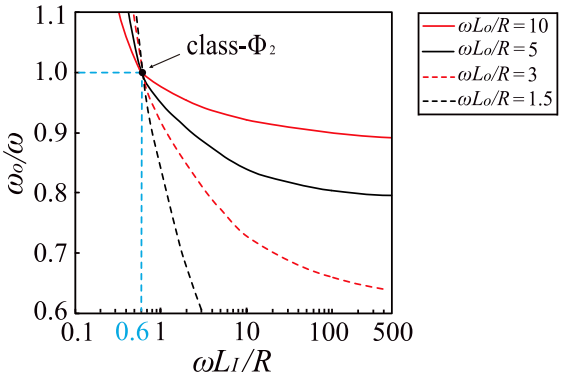

FIGURE 9. Ratio of the normalized resonant frequency of the class-E/F$_2$ inverter to obtain the c_{pmax} for fixed $\omega L_0/R$ as a function of $\omega L_I/R$.

Figure 9 shows the normalized resonant frequency ω_0/ω to obtain the highest power output capability for fixed $\omega L_0/R$ as a function of $\omega L_I/R$, where

$$\frac{\omega_0}{\omega} = \frac{1}{\sqrt{\omega L_0/R \cdot \omega C_0 R}}. \tag{29}$$

The conditions of $\omega_0/\omega > 1$ and $\omega_0/\omega < 1$ mean that the output resonant filter is capacitive and inductive, respectively. It is seen that $\omega_0/\omega = 1$ is obtained at the point of $\omega L_I/R = 0.6$ regardless of $\omega L_0/R$. From Figs. 8 and 9, it can be stated that $\omega L_I/R = 0.6$ is a particular value of the class-E/F$_2$ inverter.

As the decrease in the input inductance, a non-negligible input-current ripple occurs. This means that the class-E/F$_2$ inverter has another resonant topology with L_I and C_S. Therefore, the class-E ZVS/ZDS conditions can be achieved even though the reactance component of the output resonant filter is zero. The class-E/F$_2$ inverter, which operates at $\omega_0/\omega = 1$, is called the class-Φ_2 inverter [17], [18]. From Fig. 6(a), it can be stated that the parameter set of the class-Φ_2 inverter is one of the best parameter sets of the class-E/F$_2$ inverter in the sense of the largest output power and sufficiently high c_p.

B. CLASS-E/F$_3$ INVERTER

Figure 10 shows c_{pmax} of the class-E/F$_3$ inverter and $\omega L_3/R$ to obtain c_{pmax} for fixed $\omega L_0/R$ and $\omega L_I/R$ as a function of the duty ratio. It is seen from Fig. 10 that there is a peak of c_{pmax} for all the combinations of $\omega L_0/R$ and $\omega L_I/R$. The peaks appear at $D = 0.575$. The value of $D = 0.575$ was also pointed out in [13]. In [13], however, the power output capability was investigated under the conditions of high L_I and Q_0. It is clarified in this paper that the value of $D = 0.575$ is independent of $\omega L_I/R$ and $\omega L_0/R$. In the following investigations, the duty ratio is fixed as $D = 0.575$.

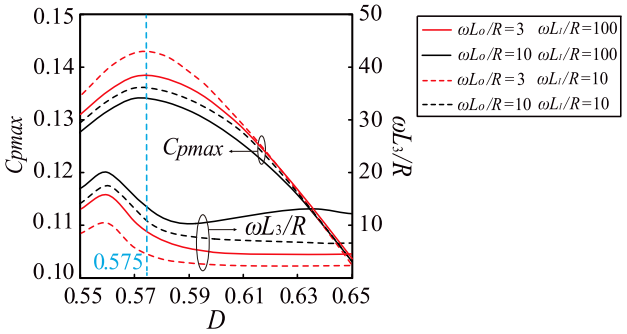

FIGURE 10. Maximum power output capability c_{pmax} of the class-E/F$_3$ inverter and $\omega L_3/R$ to obtain c_{pmax} for fixed $\omega L_I/R$ and $\omega L_0/R$ as a function of duty ratio.

1) MAXIMUM POWER OUTPUT CAPABILITY

Figure 11 shows the characteristics of the class-E/F$_3$ inverter for fixed $\omega L_I/R$ as a function of the $\omega L_0/R$. It is seen from Fig. 11(a) that the power output capability is $c_p = 0.135$ when the $\omega L_I/R$ and $\omega L_0/R$ are sufficiently large. This result is the same as that in [13]. When we consider the effects of the $\omega L_I/R$, we see that the high c_{pmax} can be obtained

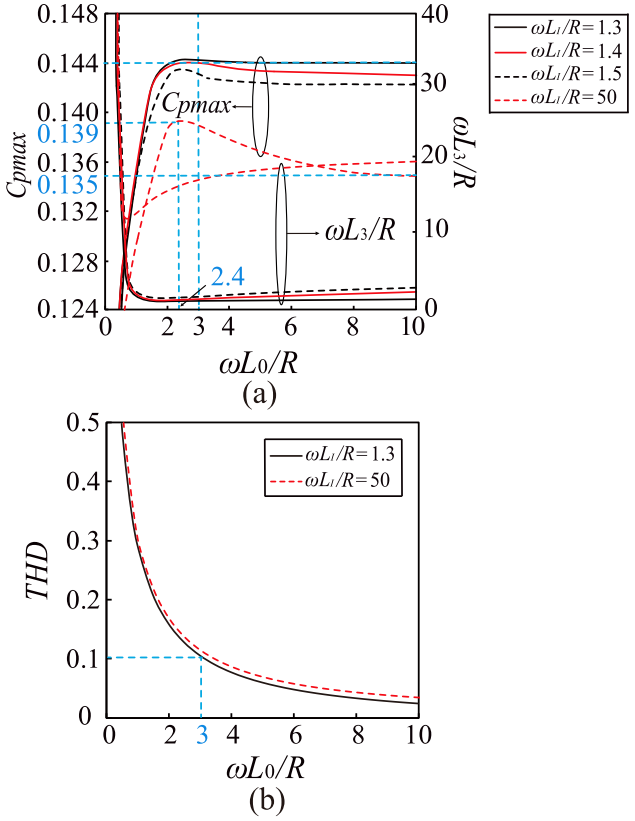

FIGURE 11. Characteristics of the class-E/F$_3$ inverter for fixed $\omega L_I/R$ as a function of the $\omega L_0/R$. (a) Maximum power output capability c_{pmax} and $\omega L_3/R$ to obtain c_{pmax}. (b) Total harmonic distortion of the output current.

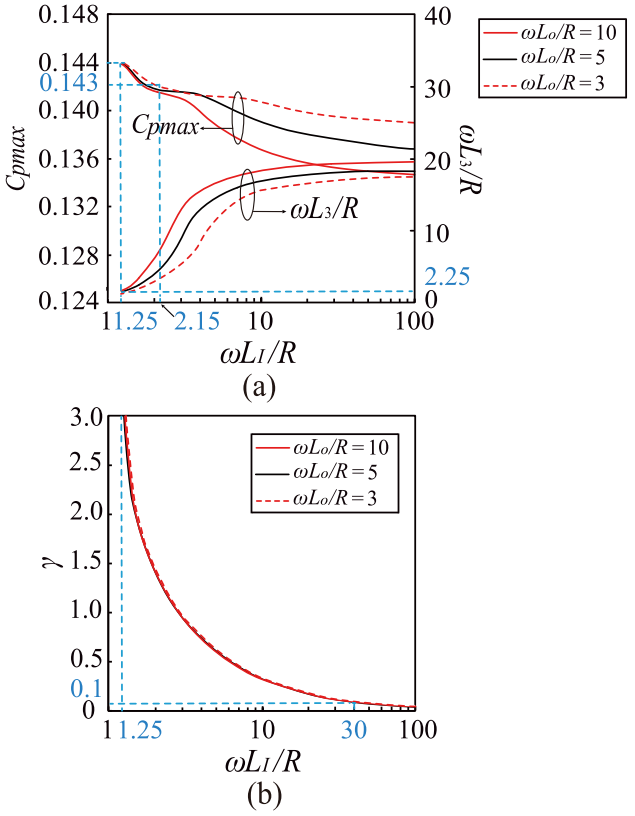

FIGURE 12. Characteristics of the class-E/F$_3$ inverter for fixed $\omega L_0/R$ as a function of the $\omega L_I/R$. (a) Maximum power output capability c_{pmax} and $\omega L_3/R$ to obtain c_{pmax}. (b) Ripple ratio of the input current.

at low $\omega L_I/R$. Namely, $c_{pmax} = 0.144$ can be obtained at $\omega L_I/R = 1.3$. The value with $c_p = 0.144$ is significantly higher than the previous-known highest value with $c_p = 0.135$, which is discovered by considering low L_I, low Q_3, and low Q_0. It is seen from Fig. 11(b) that the THD is independent of $\omega L_0/R$ and it is less than 0.1 in the range of $\omega L_0/R > 3$. Namley, $c_p = 0.144$ can be obtained at low Q_0.

Figure 12 shows the characteristic of the class-E/F$_3$ inverter for fixed $\omega L_0\, R$ as a function of the $\omega L_I/R$. It is seen from Fig. 12(a) that c_{pmax} increases as $\omega L_I/R$ decreases. The highest values of c_{pmax} appears at $\omega L_I/R = 1.25$, which is the edge of the characteristic curve. When $\omega L_I/R < 1.25$, there is no solution for achieving the class-E ZVS/ZDS conditions. From Figs. 11(a) and 12(a), the class-E/F$_3$ inverter with $c_p = 0.144$ can be designed for $D = 0.575$, $\omega L_I R = 0.125$, and $\omega L_3\, R = 2.25$ in the range of $\omega L_0/R > 2$. It is seen from Fig. 12(b) that the dc input current is provided in the range of $\omega L_I/R > 30$. Therefore, it can be stated that the input current should include large ripple for obtaining high c_p in the class-E/F$_3$ inverter, which is different from the class-E/F$_2$ inverter.

2) OUTPUT POWER AND CLASS-Φ_3 INVERTER

Figure 13 shows the normalized output power of the class-E/F$_3$ inverter to obtain c_{pmax} as a function of the $\omega L_I/R$ for the fixed $\omega L_0/R$. It is seen from Fig. 13 that there is a peak

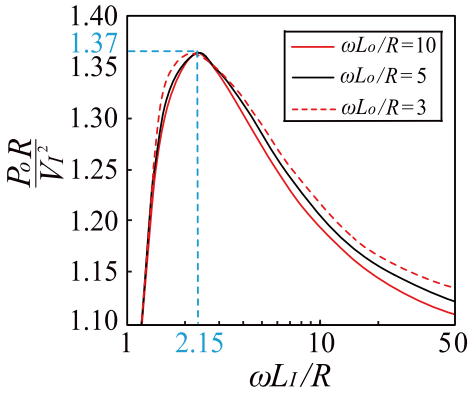

FIGURE 13. Normalized output power of the class-E/F$_3$ inverter for fixed $\omega L_0/R$ as a function of $\omega L_I/R$.

of the normalized output power at $\omega L_I/R = 2.15$. The peak value of the normalized output power is $P_o R/V_I^2 = 1.37$. It is seen from Fig. 12(a) that $c_p = 0.143$ can be obtained at $\omega L_I/R = 2.15$, which is almost the same as $c_p = 0.144$.

Figure 14 shows the normalized resonant frequency ω_0/ω for fixed $\omega L_0/R$ as a function of $\omega L_I/R$. We have $\omega_0/\omega = 1$ at $\omega L_I/R = 2.15$ regardless of $\omega L_0/R$. Similar to the class-E/F$_2$ inverter, the $\omega L_I/R$ to obtain the highest output power is the same as that for $\omega_0/\omega = 1$. From the result, the

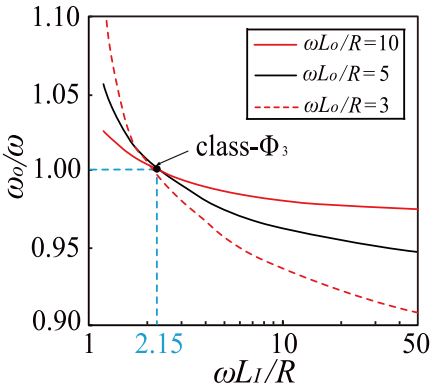

FIGURE 14. Ratio of the normalized resonant frequency of the class-E/F$_3$ inverter for fixed $\omega L_0/R$ as a function of $\omega L_I/R$.

class-Φ_3 inverter is one of the good-performed class-E/F$_3$ inverters in the sense of the largest output power and the sufficiently high c_p.

V. EXPERIMENTAL VERIFICATIONS

For confirming the validity of the analysis, the circuit experiments of four inverters were carried out in this paper. The fundamental specifications of all the inverters were: operating frequency $f = 1$ MHz, input voltage $V_I = 12$ V, and load resistance $R = 15\ \Omega$. The duty ratio is $D = 0.375$ for class-E/F$_2$ and class-Φ_2 inverter, and is $D = 0.575$ for class-E/F$_3$ and class-Φ_3 inverter. In addition, Vishay IRF510 MOSFET was chosen as the switching device. The MOSFET on-resistance was 0.54 Ω, and drain-to-source capacitance was 96 pF, which were obtained from the datasheet. Figure 15 shows the experimental prototype.

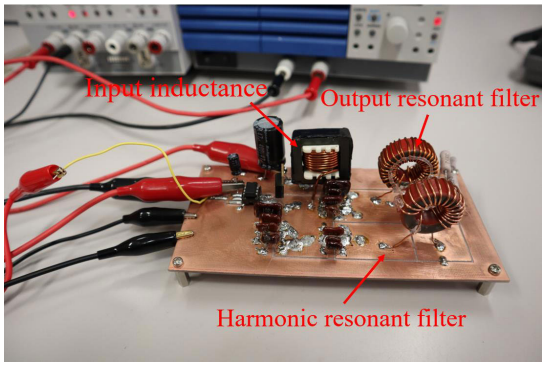

FIGURE 15. Experimental prototype of the class-E/F$_3$ inverter.

A. EXPERIMENTAL RESULTS OF CLASS-E/F$_2$ AND CLASS-Φ_2 INVERTERS

The class-E/F$_2$ inverter was designed with sufficiently large L_I and Q_0 for achieving the highest value of c_p, which was the same specifications as the previous paper in [12]. From Figs. 6(a) and 7(a), we obtained $\omega L_I/R = 100$, $\omega L_0/R = 5$, and $\omega L_2/R = 1.79$. The class-Φ_2 inverter was designed for providing $c_p = 0.132$. Figs. 7(a) and 9, we could give $\omega L_0/R = 5$, $\omega L_I/R = 0.6$, and $\omega L_2/R = 0.48$. All the component values are given in Table 2. In the experiments, the component values were measured by Keysight E4990A.

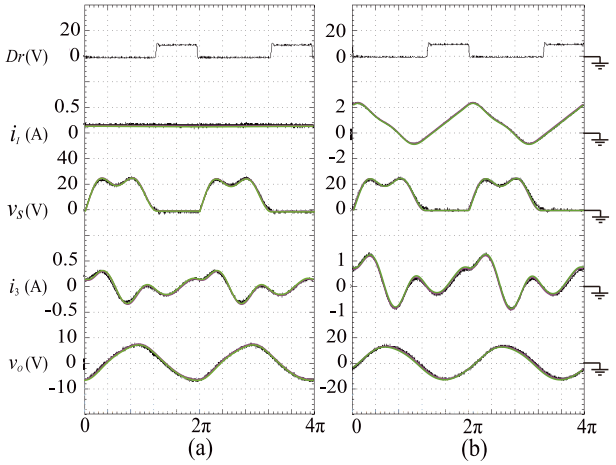

FIGURE 16. Experimental (black line), PSpice-simulation (purple line) and analytical (green line) waveforms. (a) Class-E/F$_2$ inverter. (b) Class-Φ_2 inverter.

Figure 16 shows experimental, PSpice simulation, and analytical waveforms of the class-E/F$_2$ and class-Φ_2 inverters. The experimental waveforms were measured by Tektronix MDO4043 oscilloscope. For current measurements, we used the Tektronix TCP2020 current probe. It is seen from Fig. 16(a) that the input and output currents of the class-E/F$_2$ inverter were direct current and pure sinusoidal one, respectively. Conversely, it is seen from Fig. 16(b) that the input current of the class-Φ_2 inverter includes a large ripple because of low L_I. The amplitude of the output voltage of the class-Φ_2 inverter was much larger than that of the class-E/F$_2$ inverter, which agreed with the theoretical prediction in Fig. 8. Both the switch-voltage waveforms satisfied the class-E ZVS /ZDS conditions. In the experimental measurements, the class-E/F$_2$ inverter achieved 93.2 % power-conversion efficiency at 1.53 W and 1 MHz output. The class-Φ_2 inverter achieved 92.2 % power-conversion efficiency at 7.08 W and 1 MHz output.

B. EXPERIMENTAL RESULTS OF CLASS-E/F$_3$ AND CLASS-Φ_3 INVERTERS

For the design of the class-E/F$_3$ inverter, sufficiently high L_I and Q_0 are specified, which was the same specifications as the previous paper in [13]. As stated in Section 4.2.1, we gave $\omega L_I/R = 50$, $\omega L_0/R = 10$, and $\omega L_3/R = 19.9$. The class-Φ_3 inverter was designed for achieving the $c_p = 0.143$. Therefore, $\omega L_I/R = 2.15$, $\omega L_0/R = 3$, and $\omega L_3/R = 3.11$ were given. Table 3 gives all the analytical and measured component values.

Figure 17 shows experimental, PSpice simulation, and analytical waveforms of the class-E/F$_3$ and class-Φ_3 inverters. It is seen from Fig. 17(a) that the input current was the direct current, and the currents flowing through the

TABLE 2. Analytical and measurement values of the class-E/F$_2$ and class Φ_2 inverters.

	Class E/F$_2$		Class Φ_2	
Parameters	Analytical	Experimental	Analytical	Experimental
L_I (μH)	238	235	1.43	1.43
L_2 (μH)	4.27	4.26	1.19	1.19
L_0 (μH)	12.0	12.0	12.0	12.0
C_2 (nF)	1.53	1.53	5.31	5.31
C_o (nF)	3.25	3.25	2.12	2.12
C_S (nF)	1.70	1.70	7.21	7.21
f (MHz)	1.00	1.00	1.00	1.00
D	0.375	–	0.375	–
V_I (V)	12	12	12	12
R (Ω)	15	15.0	15	15.0
r_{LI} (Ω)	0.02	0.02	0.20	0.18
r_{L2} (Ω)	0.20	0.26	0.20	0.15
r_{Lo} (Ω)	0.20	0.24	0.20	0.24
p_{out} (W)	1.59	1.53	7.17	7.08
c_p	0.133	0.130	0.132	0.130
η (%)	95.8	93.2	93.4	92.2

TABLE 3. Analytical and measurement values of the class-E/F$_3$ and class Φ_3 inverters.

	Class E/F$_3$		Class Φ_3	
Parameters	Analytical	Experimental	Analytical	Experimental
L_I (μH)	119	119	5.13	5.13
L_3 (μH)	47.6	47.5	7.42	7.41
L_0 (μH)	23.9	23.8	7.16	7.16
C_3 (pF)	59.0	58.9	379	379
C_o (nF)	1.11	1.11	3.54	3.54
C_S (nF)	1.08	1.07	1.76	1.76
f (MHz)	1.00	1.00	1.00	1.00
D	0.575	–	0.575	–
V_I (V)	12	12	12	12
R (Ω)	15	15.0	15	15.0
r_{LI} (Ω)	0.02	0.02	0.20	0.21
r_{L3} (Ω)	0.20	0.42	0.20	0.30
r_{Lo} (Ω)	0.20	0.35	0.20	0.15
p_{out} (W)	9.82	9.62	12.42	11.90
c_p	0.135	0.133	0.143	0.141
η (%)	92.5	91.0	94.5	92.5

harmonic- and output-resonant filters were pure sinusoidal waveforms.

Conversely, it is seen from Fig. 17(b) that all he currents included much harmonic components. Both the switch-voltage waveforms in Figs. 17(a) and (b) satisfied the class-E ZVS /ZDS conditions. The measured efficiency of the class-E/F$_3$ inverter was 92.0 % with 9.62 W and 1 MHz output. That of the class-Φ_3 inverter was 90.5 % with 11.9 W and 1 MHz output.

It is seen from Figs. 16 and 17 that the experimental and PSpice-simulation waveforms of all the inverters agreed with analytical waveforms perfectly. In addition, it can be also confirmed from Tables 2 and 3 that the measured values of the output power and the power output capability were also agreed with the analytical values. These results showed the validities of the analytical expressions and characteristic curves shown in this paper.

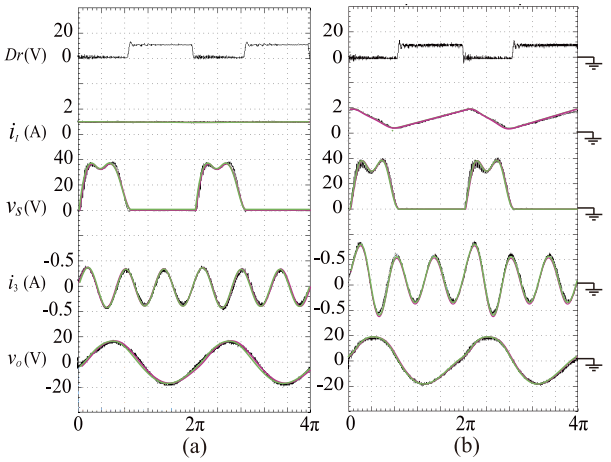

FIGURE 17. Experimental (black line), PSpice simulation (purple line) and analytical (green line) waveforms. (a) Class-E/F$_3$ inverter. (b) Class-Φ_3 inverter.

VI. CONCLUSION

This paper has presented the analytical expressions of the class-E/F$_n$ inverters. In-depth investigations of the class-E/F$_2$ and class-E/F$_3$ inverters are carried out in terms of the power output capability. From the analytical investigations, many suggestions can be obtained. The class-E/F$_2$ inverter can achieve the highest power output capability $c_p = 0.133$. Additionally, a parameter set for obtaining the highest power output capability $c_p = 0.144$ has been discovered for the class-E/F$_3$ inverter. The class-Φ_n inverter works with the highest output power of the class-E/F$_n$ inverter. Four design examples were given for the experimental verification in this paper. The experimental and PSpice-simulation results agreed with the analytical predictions quantitatively, which denoted the validities of the analytical expression and the characteristic investigations presented in this paper.

APPENDIXES

APPENDIX A

RESULTING EQUATIONS OF FOURIE SERIES EXPANSION

The resulting equations of coefficients of the Fourie series expansion are expressed as

$$\begin{aligned} c_0 &= \frac{1}{2\pi}\int_0^{2\pi} v_S\, d(\omega t) \\ &= \frac{1}{2\pi\omega C_s}\Big\{2I_c\pi^2D^2 + \sum_{k=1}^{N}\Big[\frac{A_k}{k^2}(\cos 2\pi D - 1 \\ &\quad + \frac{B_k}{k^2}\sin 2\pi D - \frac{B_n}{n}2\pi D\Big]\Big\}, \qquad (30) \\ c_k &= \frac{1}{\pi}\int_0^{2\pi} v_S \cos k\omega\, d(\omega t) \\ &= \frac{1}{\pi\omega C_s}\Big\{\frac{I_c}{k}[2\pi D\sin k2\pi D + \frac{1}{k}(\cos k2\pi D - 1)] \\ &\quad + \sum_{m=1}^{N}(-\frac{B_m}{mk}\sin k2\pi D) \end{aligned}$$

$$+\sum_{\substack{m=1,\\ m\neq k}}^{N}\Big\{-\frac{A_m}{2m}\Big[\frac{1}{m+k}[1-\cos(m+k)2\pi D]+\frac{1}{m-k}[1-\cos(m-k)2\pi D]\Big]+\frac{B_m}{2m}\Big[\frac{1}{m+k}\sin(m+k)2\pi D+\frac{1}{m-k}\sin(m-k)2\pi D\Big]\Big\}+\sum_{k=1}^{N}\Big\{-\frac{A_k}{2k}\Big[-\frac{1}{2k}\cos 4\pi D+\frac{1}{2k}\Big]+\frac{B_k}{2k}\Big[\frac{1}{2k}\sin 4\pi D+2\pi D\Big]\Big\}\Big\rangle, \tag{31}$$

and

$$\begin{aligned} d_k &= \frac{1}{\pi}\int_0^{2\pi} v_S \sin k\omega\, d(\omega t)\\ &= \frac{1}{\pi\omega C_s}\Big\langle -\frac{I_c}{k}[2\pi D\cos k2\pi D-\frac{1}{k}\sin k2\pi D]\\ &\quad+\sum_{m=1}^{N}(\frac{B_m}{mk}\cos k2\pi D-1)\\ &\quad+\sum_{\substack{m=1,\\ m\neq k}}^{N}\Big\{\frac{B_m}{2m}\Big[\frac{1}{m+k}[1-\cos(m+k)2\pi D]\\ &\quad+\frac{1}{m-k}[\cos(m-k)2\pi D-1]\Big]\\ &\quad+\frac{A_m}{2m}\Big[\frac{1}{m+k}\sin(m+k)2\pi D\\ &\quad-\frac{1}{m-k}\sin(m-k)2\pi D\Big]\Big\}\\ &\quad+\sum_{k=1}^{N}\Big\{\frac{A_k}{2k}\Big[\frac{1}{2k}\cos 4\pi D-2\pi D\Big]\\ &\quad+\frac{B_k}{2k}\Big[-\frac{1}{2k}\cos 4\pi D+\frac{1}{2k}\Big]\Big\}\Big\rangle, \end{aligned} \tag{32}$$

respectively, where

$$\begin{aligned} A_k &= a_{ik}-a_{nk}-a_{ok},\\ B_k &= b_{ik}-b_{nk}-b_{ok},\\ A_m &= a_{im}-a_{2m}-a_{om},\\ B_m &= b_{im}-b_{2m}-b_{om}. \end{aligned}$$

APPENDIX B
EXPRESSION OF POWER LOSSES

The analytical expressions of the power losses are expressed follows.

$$\begin{aligned} \frac{RP_S}{V_I^2} &= \frac{r_S}{2\pi R}\int_{2\pi(1-D)}^{2\pi}\Big(\frac{Ri_S}{V_I}\Big)^2 d(\omega t)\\ &= \frac{Dr_S a_{io}^2}{R}+\frac{r_S a_{io}}{\pi R}[-\sum_{k=1}^{N}\frac{A_k}{k}\sin(2\pi(1-D))\\ &\quad+\sum_{k=1}^{N}\frac{B_k}{k}\cos(2\pi(1-D))-\sum_{k=1}^{N}\frac{B_k}{k}]\\ &\quad+\frac{r_S}{2\pi R}\Big\langle\sum_{k=1}^{N}A_k^2[-\frac{1}{4k}\sin(4k\pi(1-D))+\pi D]\\ &\quad+\sum_{k=1}^{N}B_k^2[\frac{1}{4k}\sin(4k\pi(1-D))+\pi D]\\ &\quad+2\sum_{k=1}^{N}A_kB_k[-\frac{1}{2k}\sin^2(2\pi k(1-D))]\\ &\quad+2\sum_{k=1}^{N}\Big\{\sum_{\substack{m=1,\\ m\neq k}}^{N}A_kB_m[\frac{\cos(k+m)(2\pi(1-D))-1}{2(k+m)}]\\ &\quad+[\frac{\cos(k-m)(2\pi(1-D))-1}{2(k-m)}]\Big\}\\ &\quad+2\sum_{k=1}^{N}\Big\{\sum_{\substack{m=1,\\ m\neq k}}^{N}A_kA_m[-\frac{\sin(k-m)(2\pi(1-D))}{2(k-m)}]\\ &\quad-[\frac{\sin(k+m)(2\pi(1-D))}{2(k+m)}]\Big\}\\ &\quad+2\sum_{k=1}^{N}\Big\{\sum_{\substack{m=1,\\ m\neq k}}^{N}B_kB_m[\frac{\sin(k+m)(2\pi(1-D))}{2(k+m)}]\\ &\quad-[\frac{\sin(k-m)(2\pi(1-D))}{2(k-m)}]\Big\}\Big\rangle. \end{aligned} \tag{33}$$

$$\begin{aligned} \frac{RP_{LI}}{V_I^2} &= \frac{r_{LI}}{2\pi R}\int_0^{2\pi}\Big(\frac{Ri_I}{V_I}\Big)^2 d(\omega t)\\ &= \frac{r_{LI}}{R}\Big[a_{io}^2+\frac{1}{2}\sum_{k=1}^{N}(a_{ik}^2+b_{ik}^2)\Big]. \end{aligned} \tag{34}$$

$$\begin{aligned} \frac{RP_{Ln}}{V_I^2} &= \frac{r_{Ln}}{2\pi R}\int_0^{2\pi}\Big(\frac{Ri_n}{V_I}\Big)^2 d(\omega t)\\ &= \frac{r_{Ln}}{2R}\sum_{k=1}^{N}(a_{nk}^2+b_{nk}^2). \end{aligned} \tag{35}$$

$$\begin{aligned} \frac{RP_{Lo}}{V_I^2} &= \frac{r_{Lo}}{2\pi R}\int_0^{2\pi}\Big(\frac{Ri_o}{V_I}\Big)^2 d(\omega t)\\ &= \frac{r_{Lo}}{2R}\sum_{k=1}^{N}(a_{ok}^2+b_{ok}^2). \end{aligned} \tag{36}$$

REFERENCES

[1] M. Kazimierczuk, *RF Power Amplifiers*, 2nd ed. Chichester, U.K.: Wiley, 2015.

[2] A. Grebennikov, N. Sokal, and M. Franco, *Switchmode RF and Microwave Power Amplifiers*. Oxford, U.K.: Academic, 2012.

[3] H. Sekiya, I. Sasase, and S. Mori, "Computation of design values for class e amplifiers without using waveform equations," *IEEE Trans. Circuits Syst. I, Fundam. Theory Appl.*, vol. 49, no. 7, pp. 966–978, Jul. 2002.

[4] T. Nagashima, X. Wei, T. Suetsugu, M. K. Kazimierczuk, and H. Sekiya, "Waveform equations, output power, and power conversion efficiency for class-E inverter outside nominal operation," *IEEE Trans. Ind. Electron.*, vol. 61, no. 4, pp. 1799–1810, Apr. 2014.

[5] M. Kazimierczuk and K. Puczko, "Exact analysis of class E tuned power amplifier at any Q and switch duty cycle," *IEEE Trans. Circuits Syst.*, vol. CAS-34, no. 2, pp. 149–159, Feb. 1987.
[6] F. Raab, "Idealized operation of the class E tuned power amplifier," *IEEE Trans. Circuits Syst.*, vol. CAS-24, no. 12, pp. 725–735, Dec. 1977.
[7] N. O. Sokal and A. D. Sokal, "Class E-A new class of high-efficiency tuned single-ended switching power amplifiers," *IEEE J. Solid-State Circuits*, vol. SSC-10, no. 3, pp. 168–176, Jun. 1975.
[8] Y. Yamada, T. Nagashima, Y. Ibuki, Y. Fukumoto, T. Ikenari, and H. Sekiya, "Design of a DC-DC converter with phase-controlled class-D ZVS inverter," *IEEE J. Emerg. Sel. Topics Circuits Syst.*, vol. 5, no. 3, pp. 354–363, Sep. 2015.
[9] S. D. Kee, I. Aoki, A. Hajimiri, and D. Rutledge, "The class-E/F family of ZVS switching amplifiers," *IEEE Trans. Microw. Theory Techn.*, vol. 51, no. 6, pp. 1677–1690, Jun. 2003.
[10] A. Mediano and N. Sokal, "A class-*E* RF power amplifier with a flat-top transistor-voltage waveform," *IEEE Trans. Power Electron.*, vol. 28, no. 11, pp. 5215–5221, Nov. 2013.
[11] S. Aldhaher, D. C. Yates, and P. D. Mitcheson, "Load-independent class E/EF inverters and rectifiers for MHz-switching applications," *IEEE Trans. Power Electron.*, vol. 33, no. 10, pp. 8270–8287, Oct. 2018.
[12] S. Aldhaher, D. C. Yates, and P. D. Mitcheson, "Modeling and analysis of class EF and class E/F inverters with series-tuned resonant networks," *IEEE Trans. Power Electron.*, vol. 31, no. 5, pp. 3415–3430, May 2016.
[13] Z. Kaczmarczyk, "High-efficiency class E, EF_2, and E/F_3 inverters," *IEEE Trans. Ind Electron.*, vol. 53, no. 5, pp. 1584–1593, Oct. 2006.
[14] A. Grebennikov, "High-efficiency class E/F lumped and transmission-line power amplifiers," *IEEE Trans. Microw. Theory Tech.*, vol. 59, no. 6, pp. 1579–1588, Jun. 2011.
[15] Y. Yanagisawa, Y. Miura, H. Handa, and T. Ueda, "Characteristics of isolated DC–DC converter with class-Φ_2 inverter under various load conditions," *IEEE Trans. Power Electron.*, vol. 34, no. 11, pp. 10887–10897, Nov. 2019.
[16] J. Rivas, O. Leitermann, Y. Han, and D. Perreault, "A very high frequency DC–DC converter based on a class-Φ_2 resonant inverter," *IEEE Trans. Power Electron.*, vol. 26, no. 10, pp. 2980–2992, Oct. 2011.
[17] J. M. Rivas, Y. Han, O. Leitermann, A. D. Sagneri, and D. J. Perreault, "A high-frequency resonant inverter topology with low-voltage stress," *IEEE Trans. Power Electron.*, vol. 23, no. 4, pp. 1759–1771, Jul. 2008.
[18] L. Roslaniec, A. S. Jurkov, A. A. Bastami, and D. J. Perreault, "Design of single-switch inverters for variable resistance/load modulation operation," *IEEE Trans. Power Electron.*, vol. 30, no. 6, pp. 3200–3214, Jun. 2015.
[19] J. Phinney, D. Perreault, and J. Lang, "Synthesis of lumped transmission-line analogs," *IEEE Trans. Power Electron.*, vol. 22, no. 4, pp. 1531–1542, Jul. 2007.
[20] J. W. Phinney, D. J. Perreault, and J. H. Lang, "Radio-frequency inverters with transmission-line input networks," *IEEE Trans. Power Electron.*, vol. 22, no. 4, pp. 1154–1161, Jul. 2007.

JINGYUE MA was born in Guizhou, China, in August 1993. He received the B.E. degree in electrical engineering and automation from Beijing Jiaotong University, China, in 2016.

Since April 2017, he has been a Graduate Student with the Graduate School of Advanced Integration Science, Chiba University, Japan. His research interest is about high-frequency high-efficiency dc/ac converters.

ASIYA (Student Member, IEEE) received the B.E. degree in telecommunication engineering from Xinjiang University, Xinjiang, China, in 2003, and the M.S. degree in physical electronics from the Nanjing University of Science and Technology, China, in 2013. She is currently pursuing the Ph.D. degree with the Graduate School of Advanced Integration Science, Chiba University, Japan.

Since 2003, she has been a Lecturer with Xinjiang Normal University, Xinjiang. Her current research interest is about high-frequency high-efficiency dc/dc and ac/dc power converters and wireless power transfer systems.

XIUQIN WEI (Member, IEEE) received the B.E. degree from Fuzhou University, China, in 2005, and the Ph.D. degree from Chiba University, Japan, in 2012.

From April 2012 to October 2014, she was an Assistant Professor with the Department of Electronics Engineering and Computer Science, Fukuoka University. From November 2014 to March 2016, she was an Associate Professor with the Graduate School of Engineering, Nagasaki University. Since April 2016, she has been with the Chiba Institute of Technology, where she is currently an Associate Professor with the Department of Electrical and Electronic Engineering. Her research interests include high-frequency and high-efficiency power inverter, dc–dc converter, and wireless power transfer systems.

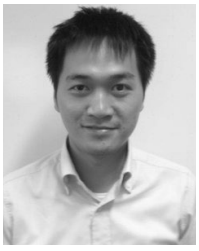

KIEN NGUYEN (Senior Member, IEEE) received the B.E. degree in electronics and telecommunication from the Hanoi University of Science and Technology (HUST), Vietnam, in 2004, and the Ph.D. degree in informatics from Graduate University for Advanced Studies, Japan, in 2012.

He is currently an Assistant Professor with the Graduate School of Engineering, Chiba University. His research includes a wide range of topics, including the Internet, the Internet of Things technologies, and wired and wireless communications. He has published more than 80 publications in peer-reviewed journals and conferences, several submitted patents, and Internet drafts.

Dr. Nguyen is a member of IEICE. He also involves in IETF activities.

HIROO SEKIYA (Senior Member, IEEE) was born in Tokyo, Japan, in July 1973. He received the B.E., M.E., and Ph.D. degrees in electrical engineering from Keio University, Yokohama, Japan, in 1996, 1998, and 2001, respectively.

Since April 2001, he has been with Chiba University, Chiba, Japan, where he is currently a Professor with the Graduate School of Engineering. His research interests include high-frequency high-efficiency tuned power amplifiers, resonant dc/dc power converters, dc/ac inverters, and digital signal processing for wireless communications.

Dr. Sekiya is a Senior Member of IEICE and a member of IPSJ and RISP, Japan.